## 1 Anhydrite Dissolution Dynamics as a Hydrogeochemical

# 2 Tracer of Seismic-Fluid Coupling: Insights from the East

## 3 Anatolian Fault Zone, Turkey

- 4 Zebin Luo<sup>1</sup>, Xiaocheng Zhou<sup>2,3</sup>, Yueren Xu<sup>2</sup>, Peng Liang<sup>2</sup>, Huiping Zhang<sup>4</sup>, Jinlong
- 5 Liang<sup>5</sup>, Zhaojun Zeng<sup>2</sup>, Yucong Yan<sup>3</sup>, Zheng Gong<sup>6</sup>, Shiguang Wang<sup>6</sup>, Chuanyou Li<sup>4</sup>,
- 6 Zhikun Ren<sup>4</sup>, Jingxing Yu<sup>4</sup>, Zifa Ma<sup>4</sup>, Junjie Li<sup>4</sup>
- 7 School of Emergency Management, Xihua University, Chengdu 610039, China
- 8 <sup>2</sup>United Laboratory of High-Pressure Physics and Earthquake Science, institute of earthquake forecasting,
- 9 CEA, Beijing 100036, China
- 3 School of Earth Sciences and Resources, China University of Geosciences, Beijing 100083, China
- <sup>4</sup>Institute of Geology, China Earthquake Administration, Beijing, 100081, China
- 5 College of Earth and Planetary Sciences, Chengdu University of Technology, Chengdu 610059, China
- 13 <sup>6</sup> Institute of Geophysics, China Earthquake Administration, Beijing, 100081, China
- 14 Correspondence to: Xiaocheng Zhou (zhouxiaocheng188@163.com).
- 15 Abstract: Pre-seismic turbidity and salinity anomalies in groundwater were documented at HS04 and
- 16 HS14 monitoring wells and/or springs along the East Anatolian Fault Zone (EAFZ) following the 2023
- 17 Mw 7.8 and Mw 7.6 Turkey earthquakes. By synthesizing hydrogeochemical datasets (2013-2023) with
- post-seismic responses, we unravel fault-segmented groundwater evolution: (1) Northern Na-Cl and Na-
- 19 HCO<sub>3</sub> type waters result from mixing of mantle-derived magmatic fluids (0-7% contribution) with
- shallow groundwater, governed by volcanic rocks-carbonate dissolution; (2) Central-southern Ca-HCO<sub>3</sub>
- 21 and Ca-Na-HCO3 systems reflect shallow circulation with localized inputs from evaporites (Increased
- $SO_4^{2-}$  concentration caused by dissolution of anhydrite), ophiolites (Mg<sup>2+</sup> anomalies), and seawater.
- 23 PHREEQC simulation shows that the dissolve-precipitation equilibrium of anhydrite is sensitive to the
- 24 variation of water-rock reaction intensity in the Central-southern segments of EAFZ. Coseismic
- 25 permeability changes disrupt the solubility equilibria of anhydrite, driving hydrochemical anomalies. We
- 26 propose that seismic stress redistribution induces fracture network reorganization, thereby disrupting
- 27 anhydrite solubility equilibria. Given its tectonic sensitivity and widespread occurrence, anhydrite
- 28 dissolution dynamics emerge as a potential tracer for hydrogeochemical monitoring in active fault zones.
- 29 We propose a novel research paradigm wherein regional hydrogeological surveys identify applicable
- 30 target indicator horizons, enabling continuous monitoring and establishment of region-specific
- 31 evaluation metrics to ultimately achieve early warning capabilities for geohazard precursors.

32 Key words: Groundwater; Water-rock interaction; Seismic activity; PHREEQC; Anhydrite; East

33 Anatolian Fault Zone.

#### 1 Introduction

34

35

36

37

38 39

40

41 42

43

44 45

46

47

48

49

50

51

52

53 54

55

56 57

58

59

Active fault zones perturb subsurface hydrogeochemical equilibrium through dynamic rock-water interactions, generating diagnostic anomalies in groundwater chemistry that may serve as potential seismic precursors (Franchini et al., 2021; Ingebritsen and Manga, 2014; King et al., 2006; Luo et al., 2023; Poitrasson et al., 1999; Skelton et al., 2014; Tsunogai and Wakita, 1995; Wang et al., 2021). However, the diagnostic reliability of such hydrochemical signatures faces challenges. Climatic factors (e.g., precipitation variability and temperature fluctuations) can mask tectonic signals by altering waterrock reaction kinetics (Okan et al., 2018), while regional heterogeneity in lithology, fracture density, and hydrological circulation depth introduces substantial spatial variability in groundwater (Luo et al., 2023). This study investigates the hydrogeochemical characteristics of the seismically active East Anatolian Fault Zone (EAFZ) in eastern Turkey through a comprehensive 13-year observational dataset (2013-2023). By systematically analyzing groundwater circulation patterns and water-rock interaction processes along the fault system, we integrate post-seismic hydrochemical monitoring following the February 2023 Mw 7.8 and 7.6 earthquake sequence to delineate the relationship between hydrogeochemical anomalies and fault activity. Our findings aim to establish the relationship between groundwater anomalies and fault zone activities, thereby advancing methodologies for groundwaterbased seismic monitoring in active fault zone systems. The EAFZ, a ~500 km NE-SW trending left-lateral strike-slip system accommodating ~11 mm/yr of Anatolian-Arabian plate motion with reverse thrust components (Pousse - Beltran et al., 2020), has generated destructive seismic events throughout recorded history (Hubert-Ferrari et al., 2020; Simão et al., 2016; Sparacino et al., 2022; Tan et al., 2008). The 2023 twin earthquakes exemplify its capacity for massive stress release (Kwiatek et al., 2023; Ma et al., 2024; Wang et al., 2023b), producing coseismic surface ruptures exceeding 280 km with maximum slip of 7.2±0.72 m (Liang et al., 2024). Notably, marked hydrochemical anomalies (e.g., white water, turbidity and intermittent groundwater gushing) were detected at monitoring spring HS04 and well HS14 both before and after the earthquake (Video 1

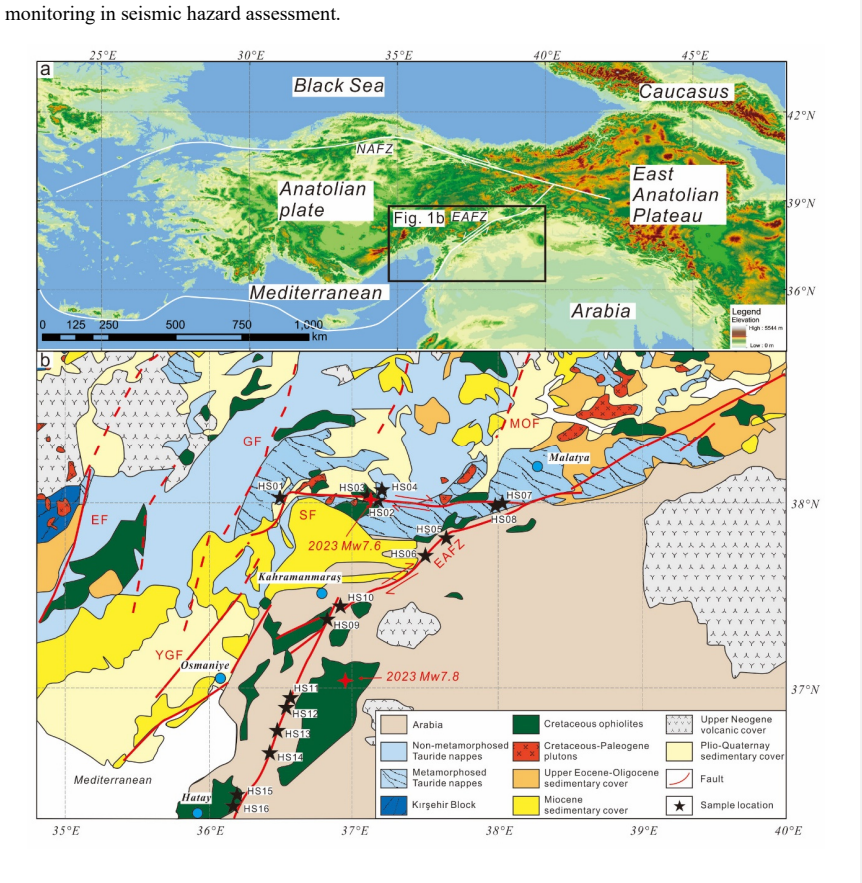
删除了: wells HS04 and HS14

and 2), indicating fault-controlled fluid responses to seismic stress perturbations.

Previous studies have identified three primary fluid sources within the EAFZ system: 1) mantle-derived magmatic fluids (Aydin et al., 2020; Italiano et al., 2013; Karaoğlu et al., 2019), 2) deeply circulated metamorphic waters (Yuce et al., 2014), and 3) Mediterranean seawater intrusion at its southern terminus (Yuce et al., 2014). These studies provide sufficient data support for accurate understanding of EAFZ groundwater circulation. In this contribution, the EAFZ groundwater observation data over the past 13 years are compared with the groundwater chemical composition after the double earthquakes in 2023 to tracing the origin of groundwater, restore the water-rock interaction process, and evaluate the influence of seismic activity on the groundwater, circulation process. We have proposed that an abnormality in groundwater chemical components, which does not require the involvement of deep fluids, could potentially serve as a basis for earthquake prediction. It provides new constraints on tectonic controls of deep fluid migration in active fault zone systems while advancing the application of hydrogeochemical

删除了: geothermal fluid 删除了: geothermal fluid

删除了: This work



- 77 Fig. 1. a: A brief Map of the eastern Mediterranean region from NASADEM
- 78 (https://doi.org/10.5069/G93T9FD9). b: Geological map of EAFZ, modified from (van Hinsbergen et al.,
- 79 2024). EF: Ecemiş Fault, SF: Sürgü Fault, MOF: Malatya-Ovacık Fault, GF: Göksün Fault, YGF: Yeşilgöz-
- 80 Göksün Fault.

81

#### 2 Geologic background

- Located at the intersection of Eurasia, Africa and Arabia, Turkey has a complex tectonic background
   (Lanari et al., 2023; Simão et al., 2016). Here, the collision between the Arabian and Eurasian plates was
   an important tectonic process that began in the early Miocene (~ 23 Ma) and continues to the this day
- 85 (van Hinsbergen et al., 2024). This collision caused plateau uplift, volcanic eruptions, sedimentary basin
- 86 formation, and large-scale strike-slip faults in eastern Turkey, including the EAFZ (Fig. 1) (Bilim et al.,
- 87 2018; Karaoğlu et al., 2018; Karaoğlu et al., 2020; Whitney et al., 2023; Yönlü et al., 2017; Zhou et al.,
- 88 2024).
- 89 The formation of the EAFZ is related to the northward subduction of a strong and thin lithospheric wedge
- 90 under the Arabian Plate (Nalbant et al., 2002; Sparacino et al., 2022). This subduction process led to the
- 91 formation of a stress concentration zone that eventually developed into a strike-slip fault that penetrated
- 92 the entire lithosphere, i.e. the EAFZ (Nalbant et al., 2002). In addition, because the African plate and the
- Arabian plate are still moving northward, this fault zone is also accompanied by a certain thrust process,
- 94 which causes huge stresses at the plate margin (Ma et al., 2024; Över et al., 2023; Özkan et al., 2023;
- 95 Pousse Beltran et al., 2020; Wang et al., 2023b; Whitney et al., 2023).
- 96 The stratigraphic composition of the East Anatolian fault zone is complex, including Non-
- 97 metamorphosed Tauride nappes and Metamorphosed Tauride nappes crystallization base, Cretaceous
- 98 ophiolites and Cretaceous-Paleogene plutons. It is overlaid by clastic deposits, lacustrine deposits (such
- 99 as: Ancient Amik Lake) and volcanic cover of Upper Eocene-Oligocene to Plio-Quaternay. Faults are
- widely developed in study area, including East Anatolian Fault, Ecemiş Fault, Sürgü Fault, Malatya-
- 101 Ovacık Fault, Göksün Fault, Yeşilgöz-Göksün Fault etc. (van Hinsbergen et al., 2024). These faults has
- been active for a long time and has a history of devastating earthquakes, including two in February 2023
- 103 (Mw 7.8 and Mw 7.6) (Fig. 1) (Carena et al., 2023; Kwiatek et al., 2023; Ma et al., 2024; Maden and Özt
- 104 ürk, 2015; Över et al., 2023; Özkan et al., 2023; Pousse Beltran et al., 2020; Tan et al., 2008; Wang et
- 105 al., 2023b).

The climate of the EAFZ is mainly a temperate continental climate with cold winters and hot and dry summers. The average annual rainfall is between 200 mm and 600 mm, and is mainly winter rain. Due to its inland location and low rainfall, the flow of the river is relatively small. The groundwater system is relatively complex, and geothermal resources are mainly distributed near the fault zone and its controlled areas, including low or moderate temperature geothermal systems, which have great potential for development and utilization (Aydin et al., 2020; Güleç and Hilton, 2016; Inguaggiato et al., 2016; Karaoğlu et al., 2019).

### 3 Sampling and analytical methods

106

107

108

109

110

111

112

113

114

115116

117

118

119

120

121

122

123

124 125

126

127

128

129

130

131

132 133 16 samples of groundwater were collected in EAFZ, including hot springs, geothermal wells and river water. HS01-HS04 was collected from west to east along SF. HS07-HS16 was collected from north to south along EAFZ (Fig. 1). Detailed sample collection and testing methods can be found at Luo et al. (2023). In short, the water sample was taken with a 50 mL clean polyethylene bottle and the temperature and pH of the water were measured and recorded. Two samples were collected at each sampling site, one was added with ultrapure HNO3 to analyse the cation content, and the other was used to analyse the anion content and isotopic composition. All samples need to be pre-treated with a 0.45 µm filter membrane to remove impurities before sampling. The Hydrogen and oxygen isotopes were determined by a Picarro L2140-I Liquid water and vapor isotope analyzer (relative to Vienna Standard Mean Ocean Water (V - SMOW)). Precisions on the measured  $\delta^{18}O$  and  $\delta D$  value was  $\pm 0.2\%$  (2SD) and  $\pm 1\%$  (2SD) respectively (Zeng et al., 2025). The cation (Li<sup>+</sup>, Na<sup>+</sup>, K<sup>+</sup>, Ca<sup>2+</sup>and Mg<sup>2+</sup>) and anion (F<sup>-</sup>, Cl<sup>-</sup>, NO<sub>3</sub><sup>-</sup> and SO<sub>4</sub><sup>2-</sup>) were analysed by Dionex ICS-900 ion chromatograph (Thermo Fisher Scientific Inc.) at the Earthquake Forecasting Key Laboratory of China Earthquake Administration, with the reproducibility within  $\pm 2\%$  and detection limits 0.01 mg/L (Chen et al., 2015). HCO<sub>3</sub><sup>-</sup> and CO<sub>3</sub><sup>2</sup>- was determined by acid-base titration with a ZDJ-100 potentiometric titrator (reproducibility within  $\pm 2\%$ ). SiO<sub>2</sub> were analysed by inductively coupled plasma emission spectrometer Optima-5300 DV (PerkinElmer Inc.) (Li et al. 2021). Trace elements were analysed by Element XR ICP-MS at the Test Center of the Research Institute of Uranium Geology. Multielement standard solutions (IV-ICPMS 71A, IV-ICP-MS 71B and IV-ICP-MS 71D, iNORGANIC VENTURES) used for quality control. The analytical error margin of major cations and trace elements

were less than 10%. Strontium isotope ratios (87Sr/86Sr) were determined through triple quadrupole ICP-MS (Agilent 8900 ICP-QQQ) with a precision of ±0.001 (Liu et al., 2020).

#### 4 Results

Physical, chemical and isotopic compositions of groundwaters are listed in Table 1. The variation range of EC is 275 - 2683 μs/cm. The pH of the water samples varied from 7.03 to 11.72, and all the samples showed weakly alkaline characteristics except HS15 (pH=11.72). The effluent temperature of water sample is low (8.1–32.0°C), and the highest temperature is HS15 sample (32.0°C). HS08 is a river sample with the lowest temperature (8.1°C). The differences in temperature between the samples reflect specific hydrological processes. SiO<sub>2</sub> varies from 0.38 mg/L to 84.64mg/L. HCO<sub>3</sub><sup>-</sup> (165.72–1854.30 mg/L) is the main anion. The concentration of SO<sub>4</sub><sup>2-</sup> range from 1.21 mg/L to 316.61 mg/L, and the concentration of SO<sub>4</sub><sup>2-</sup> in some samples is relatively high (e.g. HS01 (287.74 mg/L), HS03 (103.56 mg/L), HS04 (229.75 mg/L), HS14 (316.61 mg/L)). The concentration of Na<sup>+</sup> (0.42–88.93 mg/L), Cl<sup>-</sup> (0.97–75.92 mg/L) and B (3.62–1047.25 μg/L) varied synergistically. Ca<sup>2+</sup> (14.16–501.58 mg/L) is the main cation, followed by Mg<sup>2+</sup> (0.38–116.20 mg/L). The types of groundwater include Na-Cl-HCO<sub>3</sub>, Ca-HCO<sub>3</sub>, Ca-HCO<sub>3</sub>-SO<sub>4</sub> and Mg-HCO<sub>3</sub> (Fig. 2 and Fig.S1). The δ<sup>18</sup>O and δD of samples varied from –11.30‰ to –6.55‰ and –65.43‰ to –34.43‰ respectively, which is near to the global meteoric water line (GMWL) (Craig, 1961) (Fig. 3), suggesting their meteoric water origin. The <sup>87</sup>Sr/<sup>86</sup>Sr varied from 0.7053 to 0.7135, showing the characteristics of multi-source region mixing.

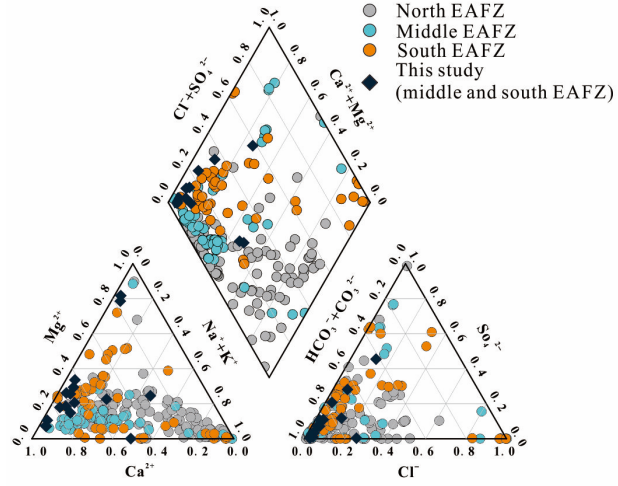


Fig. 2. Piper plot of sampled groundwaters in EAFZ. The groundwaters are Na-Cl-HCO<sub>3</sub>, Ca-HCO<sub>3</sub>, Ca-HCO<sub>3</sub>-SO<sub>4</sub> and Mg-HCO<sub>3</sub> types. Literature data source (see Table S1 for details): (Aydin et al., 2020; Baba et al., 2019; Karaoğlu et al., 2019; Okan et al., 2018; Pasvanoglu, 2020; YASİN and YÜCE, 2023; Yuce et al., 2014)

affected by human activities.

The composition of trace elements in groundwaters are shown in Table 2. The contents of Sr (30.13–3244.88 μg/L) and Ba (1.89–196.48 μg/L) in the samples varied widely. Moreover, Sr and SO<sub>4</sub><sup>2-</sup> had obvious positive correlation. Box plot analysis showed that the Fluid-Mobile Element (FME) concentrations of B (3.62–1047.25 μg/L), Li (0.33–89.93 μg/L) and Rb (0.14–28.91 μg/L) in some samples were greater than the median (Fig. S2). Enrichment coefficients (EF) normalized by Ti is used for groundwaters and rocks. The result shows that whether compared with schist, basalt or Andesite of EAFZ, trace elements in groundwaters are all in a state of enrichment, and some elements can even be enriched 100000 times (Fig. S3). The distribution patterns of trace elements in all water samples maintained a good consistency, and no abnormal changes in trace elements in specific areas (such as Pb)

were observed (Fig. S3). This indicates that the circulation of regional groundwater is only minimally

删除了: S2

删除了: S1

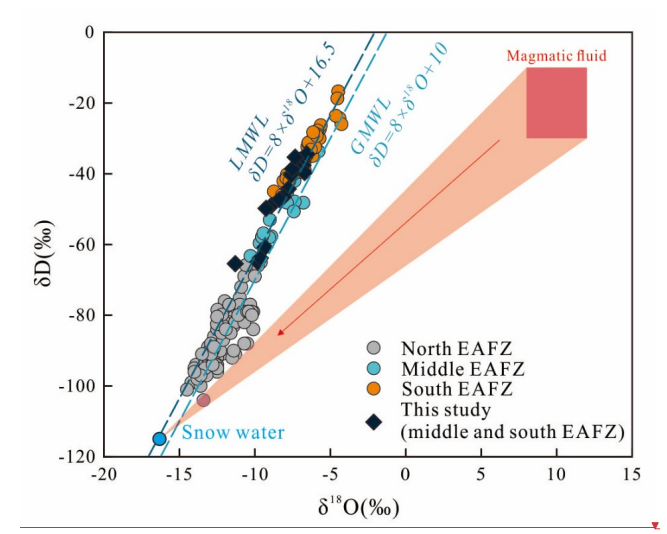


Fig. 3.  $\delta D$  and  $\delta^{18}O$  (‰V-SMOW) values for groundwaters collected from EAFZ. The GMWL represents the global meteoric water line (Craig, 1961). The LMWL represents the Local meteoric water line (Aydin et al., 2020). The magmatic fluid distribution ( $\delta D = -20 \pm 10\%$ ,  $\delta^{18}O = 10 \pm 2\%$ ) from (Giggenbach, 1992). Literature data source is consistent with Fig. 2.

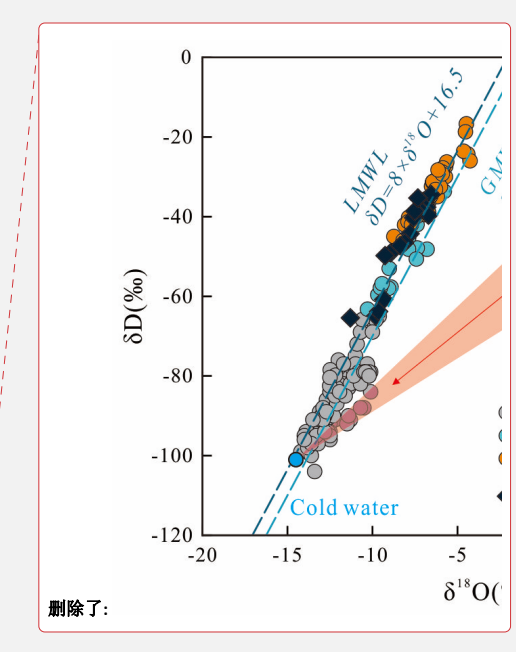


Table 1.Physical, Chemistry and isotopic compositions of groundwaters from the EAFZ.

No	Long (E)	lat (N)	Type	Date	Т	nU .	EC	SiO <sub>2</sub>	Li <sup>+</sup>	Na <sup>+</sup>	K <sup>+</sup>	$Mg^{2+}$	Ca <sup>2+</sup>	F-	Cl-	NO <sub>3</sub> -	SO <sub>4</sub> <sup>2</sup> -	HCO <sub>3</sub> -	CO3 <sup>2-</sup>	δD	δ <sup>18</sup> O	<sup>87</sup> Sr/ <sup>86</sup> S	·>5	<del></del> 设置了格式:	字体颜色: 红色	
110	(°)	(°)	Type	Date	(°C)	pm	(µS/cm)	(mg/L)	(mg/L)	(mg/L)	(mg/L)	(mg/L)	(mg/L)	(mg/L)	(mg/L)	(mg/L)	(mg/L)	(mg/L)	(mg/L)	<u>(%)</u>	_(‰)	r_			字体颜色: 红色	$\overline{}$
H\$01	36.518113	38.003517	S	03/23/2023	15.8	8.12	1565	20.70	-	27.93	4.85	75.69	253.85	3.60	55.46	-	287.74	670.01	-	<b>€</b> 64.93_	9.81_	0.7065	0.0		字体颜色: 红色	$\overline{}$
H\$02	37.173212	38.028567	S	03/23/2023	13.2	8.35	287	5.27	-	0.42	-	6.58	54.04	0.40	1.33	5.06	6.37	178.53	-	€65.43_	11.30_	0.7120	0.0	设置了格式:	字体颜色: 红色	$\overline{}$
H\$03	37.166040	38.031327	S	03/23/2023	13.2	7.12	1876	26.36	0.13	48.44	0.48	74.20	368.42	0.50	30.85	30.13	103.56	1271.1	-	<b>▲</b> 6 <u>0.7</u> 7_	9.33_	0.7079	0.0		字体颜色: 红色	$\overline{}$
H\$04	37.174886	38.033718	S	03/23/2023	15.0	7.03	2683	84.64	0.05	19.90	0.46	116.20	501.58	3.70	9.29	3.33	229.75	1854.3	-	<b>▲</b> 6 <u>3</u> .82_	9.64_	_ 0.7132	0.0	ann .	字体颜色: 红色	$\overline{}$
H\$05	37.669088	37.809271	S	03/23/2023	12.7	8.50	634	14.42	-	7.66	0.39	25.88	103.61	0.53	4.43	12.92	29.75	367.72	-	44.29_	7.79_	0.7091	0.0	ana .	字体颜色: 红色	$\overline{}$
H\$06	37.510811	37.700516	S	03/23/2023	15.0	8.27	774	15.34	-	4.19	0.32	54.08	100.99	0.43	5.98	1.61	7.96	515.66	-	46.53	8.11_	0.7100	0.0	<u> </u>	字体颜色: 红色	$\overline{}$
H\$07	38.056844	37.942560	S	03/23/2023	9.8	8.46	276	9.41	-	0.84	-	4.62	55.11	0.41	0.97	2.74	5.00	167.86	-	<b>▲</b> 49.09_	8.93_	0.7135	0.0	· · · · · · · · · · · · · · · · · · ·	字体颜色: 红色	$\overline{}$
H\$08	38.051818	37.939222	R	03/23/2023	8.1	8.43	275	15.15	-	1.13	-	4.47	55.34	0.44	1.06	3.83	5.69	165.72	-	<b>▲</b> 4 <u>9.8</u> 1_	9.26_	0.7104	0.0	· · · ·	字体颜色: 红色	$\longrightarrow$
H\$09	36.808379	37.349742	S	03/23/2023	18.0	8.11	699	25.50	0.01	5.85	0.21	42.60	94.99	0.52	6.80	8.87	93.44	344.96	-	<b>▲</b> 3 <u>7.6</u> 5_	6.81_	0.7076	0.0	···	字体颜色: 红色	$\longrightarrow$
H\$10	36.994384	37.460028	S	03/23/2023	20.0	8.48	659	31.29	-	1.57	-	90.13	18.22	0.35	3.80	7.53	2.76	459.47	-	€39.65_	<u>-6</u> .71_	_ 0.7119	0.0		字体颜色: 红色	$\longrightarrow$
H <b>\$</b> 11	36.554302	36.892454	S	03/23/2023	16.3	8.27	517	9.69	-	2.32	0.09	27.89	75.25	0.45	4.39	9.25	12.11	312.24	-	<b>₹</b> 40.30_	<u>7</u> . <u>5</u> 8_	0.7107	0.0	···	字体颜色: 红色	$\longrightarrow$
H\$12	36.521328	36.811041	S	03/23/2023	16.9	8.32	489	46.50	-	2.11	-	60.76	14.16	0.52	6.13	14.55	4.27	307.98	-	<b>∡</b> 3 <u>4.4</u> 3_	6.55_	_ 0.7110	0.0		字体颜色: 红色	$\longrightarrow$
H\$13	36.439440	36.672020	S	03/23/2023	18.2	8.22	579	10.05	0.01	4.87	0.49	30.35	81.56	0.50	7.67	8.67	39.89	309.40	-	<b>∡</b> 3 <u>7.88</u> _	7.30_	0.7080	0.0			$\longrightarrow$
H\$14	36.373823	36.503634	W	03/23/2023	23.5	8.21	1305	36.64	0.09	62.40	5.79	65.12	151.43	4.33	75.92	34.60	316.61	300.15	-	<b>∡</b> 3 <u>8.6</u> 1_	<u>-7.51</u>	0.7053	0.0		字体颜色: 红色	$\longrightarrow$
H\$15	36.163672	36.383335	S	03/23/2023	32.0	11.7	589	0.38	0.02	48.64	1.42	0.38	55.55	0.41	48.71	5.28	1.21	-	154.61	<b>▲</b> 4 <u>7.2</u> 7_	8.37_	0.7070	0.0	~~	字体颜色: 红色	$\longrightarrow$
H\$16	36.147159	36.273720	S	03/23/2023	24.5	8.45	1100	32.57	0.01	88.93	18.68	59.60	73.35	0.72	67.11	43.51	75.90	484.37	-	<b>∡</b> 3 <u>5</u> .3 <u>4</u> _	7.33	0.7073	0.0		字体颜色: 红色	$\longrightarrow$
17	7 Note: "	-" represents	helow d	etection limit	or undet	ected "	S" is Spring	"W" is V	Vell water	"R" is riv	er water													设置了格式:	字体颜色: 红色	

删除了: "S" is Hot spring

**设置了格式:**字体颜色:自动设置

9 Table 2. Trace elements compositions of groundwaters from the EAFZ.

No	В	Al	P	Sc	Ti	V	Mn	Fe	Co	Ni	Ga	Rb	Sr	Y	Zr	Nb	Ba	Hf	Ta	Pb	Th	U
NO	(µg/L)	(µg/L)	(µg/L)	(µg/L)	(µg/L)	(µg/L)	(µg/L)	(µg/L)	(µg/L)	(µg/L)	(µg/L)	(µg/L)	(µg/L)	(µg/L)	(µg/L)	(µg/L)	(µg/L)	(µg/L)	(µg/L)	(µg/L)	(µg/L)	(μg/L)
HS01	35.49	10.02	66.41	0.04	0.20	0.23	369.58	34.43	0.40	3.40	0.03	1.68	1231.40	0.04	0.19	0.02	77.45	0.004	0.01	0.19	0.001	3.15
HS02	3.62	8.26	8.94	0.02	0.22	0.85	0.73	21.10	0.01	0.16	0.04	0.25	99.69	0.01	-	0.02	16.12	-	0.01	0.14	-	0.43
HS03	1047.25	8.23	11.86	0.08	0.19	0.56	0.80	23.29	0.03	4.22	0.04	5.95	691.57	0.01	0.01	0.01	5.52	0.001	0.01	0.10	-	1.32
HS04	512.31	6.75	12.88	0.58	0.22	0.19	890.21	563.31	4.06	19.67	0.01	28.91	1505.17	0.12	0.66	0.02	11.28	0.004	0.01	0.13	0.003	0.23
HS05	43.88	6.88	9.14	0.04	0.17	2.23	0.90	16.14	0.04	0.88	0.04	0.31	667.55	0.02	0.03	0.01	196.48	0.001	0.01	0.17	-	1.64
HS06	18.60	4.50	8.79	0.03	0.18	2.74	0.67	13.54	0.02	6.23	0.01	0.37	213.59	0.02	0.03	0.01	38.11	0.001	0.01	0.15	-	0.51
HS07	8.32	12.99	10.51	0.01	0.20	2.09	3.58	81.59	0.02	0.37	0.11	0.49	53.27	0.03	0.01	0.01	3.48	-	0.01	0.26	0.004	0.32
HS08	4.77	12.27	8.89	0.03	0.18	2.85	1.05	12.52	0.02	0.26	0.01	0.44	55.78	0.06	-	0.01	1.89	-	-	0.10	-	0.26
HS09	24.05	8.48	4.56	0.04	0.27	0.50	0.99	45.62	0.01	0.81	0.02	0.62	967.07	0.02	-	0.01	105.53	-	-	0.15	-	0.49
HS10	14.56	8.37	9.74	0.03	0.23	0.73	0.62	19.86	0.02	0.68	0.01	0.19	96.74	0.06	-	-	7.85	-	-	0.16	-	0.02
HS11	9.13	8.17	13.04	0.02	0.18	0.64	2.58	134.71	0.03	2.05	0.01	0.36	263.61	0.02	0.01	0.01	22.37	0.001	-	0.11	-	0.53
HS12	7.37	28.55	23.54	0.03	0.30	1.24	2.51	49.33	0.14	5.73	0.05	0.14	34.78	0.09	-	-	38.75	-	-	0.18	0.001	0.03
HS13	14.94	10.65	10.86	0.02	0.47	0.60	15.09	805.45	0.07	1.27	0.05	0.96	592.95	0.02	0.01	0.01	146.07	-	-	0.17	-	1.01
HS14	183.76	17.48	7.06	0.07	0.14	2.50	2.94	12.72	0.04	11.66	0.00	11.25	3244.88	0.02	0.02	0.01	92.96	0.001	0.01	0.10	0.001	0.34
HS15	4.34	5.41	6.85	0.03	0.19	0.03	0.69	14.15	0.01	0.32	0.00	1.86	30.13	0.01	-	-	2.36	-	-	0.15	-	0.01
HS16	491.19	6.67	812.91	0.03	0.29	7.20	0.89	34.78	0.10	10.68	0.00	2.23	738.82	0.02	0.02	-	39.83	0.001	0.01	0.20	0.002	5.08

Note: "-" represents below detection limit or undetected. Hf and Ta are kept to 3 decimal places due to their low content.

# 5 Discussion

181

184

187

207

208

182 5.1 The origin of groundwater in different segments of EAFZ 183 Previous studies have documented abundant geothermal resources within the EAFZ, which is characterized by low or moderate temperature geothermal systems (Aydin et al., 2020; Baba et al., 2019). 185 Both aqueous and gaseous geochemical signatures indicate mixing between deep-sourced mantle/crustal fluids and shallow groundwater reservoirs (Aydin et al., 2020; Italiano et al., 2013; Yuce et al., 2014). 186 Yuce et al. (2014) proposed that geothermal fluids at the southwest end of the EAFZ are triggered by 188 deep-rooted regional faults, with localized seawater intrusion. Analogously, there are deep components 189 involved in the geothermal fluid circulation in the middle to east section of EAFZ. However, the source of deep components are thought to be controlled by magmatic activity rather than from deep-rooted 190 191 regional faults (Aydin et al., 2020; Italiano et al., 2013; Karaoğlu et al., 2019). At the intersection of the 192 EAFZ and the North Anatolian Fault Zones (NAFZ), which is also known as the Karliova triple junction, 193 there is extensive volcanic activity that may have provided energy and components for the geothermal 194 fluid cycle eastern segment of the EAFZ (Bilim et al., 2018; Karaoğlu et al., 2018; Karaoğlu et al., 2020). 195 Furthermore, Italiano et al. (2013) suggested these volcanic activities may even contribute to geothermal 196 fluids in the middle segment of the EAFZ. These findings collectively suggest multiple tectonic controls 197 (volcanism, fault activity, and seawater intrusion) on EAFZ's geothermal systems. 198 The February 2023 earthquake sequence (Mw 7.8 and 7.6) ruptured the central EAFZ segment. A critical 199 question arises: Are the observed pre-seismic groundwater anomalies (white water, turbidity and 200 intermittent groundwater gushing) (Video 1 and Video 2) seismogenically linked to this seismic event? 201 To address this, we conducted comparative analyses of post-seismic hydrochemical data against a 202 decadal-scale (13-year) pre-seismic groundwater dataset, as detailed below: 203 5.1.1 Hydrogen and oxygen isotope characteristics of groundwaters 204 Hydrogen and oxygen isotopes serve as robust geochemical tracers for elucidating the origin of 205 geothermal fluids groundwater. As illustrated in Fig. 3, the  $\delta D$  and  $\delta^{18}O$  compositions of groundwater in 206 the EAFZ align closely with the GMWL (Craig, 1961), indicating predominant atmospheric precipitation recharge. Notably, groundwater in the southern EAFZ proximal to the Mediterranean Sea exhibits

progressively heavier isotopic signatures toward the coast, consistent with recharge sourced from

evaporated Mediterranean seawater. In contrast, some northern groundwater displays distinct  $\delta^{18}O$ enrichment deviating from local meteoric trends, indicative of mixing with deep-sourced magmatic fluids—a interpretation corroborated by widespread Quaternary volcanic activity in the northern sector (Fig. 3) (Bilim et al., 2018; Karaoğlu et al., 2018; Karaoğlu et al., 2020). Conversely, central and southern groundwater samples exhibit isotopic signatures decoupled from magmatic inputs, reflecting the absence of active deep-seated magma reservoirs in these segments. 5.1.2 Major ion characteristics of groundwaters The groundwater chemistry exhibits distinct spatial heterogeneity across the EAFZ segments. Northern groundwaters are significantly enriched in Na<sup>+</sup>, K<sup>+</sup>, and Cl<sup>-</sup> (Na-Cl and Na-HCO<sub>3</sub> type), whereas central and southern segments display Ca-Mg-HCO3 type waters, with localized Ca-SO4 and Na-Cl anomalies (Fig. 2). These hydrochemical disparities likely reflect fundamentally distinct recharge sources and circulation pathways. As discussed earlier, magmatic fluid contributions are evident in northern groundwaters. Chloride serves as a key tracer for magmatic input (Luo et al., 2023; Pan et al., 2021). In the eastern EAFZ, Clconcentrations span 0.4-2500 mg/L, markedly higher than central/southern values. Given the segment's inland setting, seawater intrusion is negligible, suggesting Cl- enrichment primarily originates from magmatic fluids. Notably, Na<sup>+</sup>/Cl<sup>-</sup> molar ratios deviate from theoretical mixing trends, with Na<sup>+</sup> excesses implicating additional sodium sources (e.g., albite dissolution), to be detailed in Section 5.2. This interpretation aligns with petrological and geophysical evidence of active magmatism in the eastern EAFZ (Bilim et al., 2018; Karaoğlu et al., 2018; Karaoğlu et al., 2020; Maden and Öztürk, 2015; Oyan, 2018). Integrated H-O isotopic, major ion, and volcanic activity data collectively support a mixing model between meteoric water and magmatic fluids in the northern EAFZ. In contrast, central and southern groundwaters exhibit lower Na+ and Cl- concentrations, with sporadic anomalies attributable to evaporite dissolution or limited seawater influence (Table 1). The Ca-Mg-HCO3 dominance, coupled with isotopic signatures, reflects shallow circulation systems (<5 km depth) devoid of significant deep tectonic/magmatic inputs (Table S2). Ca2+ likely derives from calcite, dolomite, or plagioclase weathering, while Mg2+ sources include dolomite and serpentinite. Pre-seismic turbidity at HS14 (Video 1) may indicate earthquake-induced disruption of water-rock equilibria.

209

210

211

212

213

214

215

216

217

218

219220

221222

223

224

225226

227

228

229

230

231

232

233

234235

However, the geothermal gases in the centre and south segment of EAFZ exhibit mantle-like δ<sup>13</sup>C<sub>CO2</sub> (-5.6% to -0.2%) and elevated  ${}^{3}\text{He}/{}^{4}\text{He ratios}$  (Rc/Ra = 0.44-4.41), contrasting with the absence of deep fluid signatures in groundwater (Italiano et al., 2013). Actually, this decoupling results from fundamentally distinct migration mechanisms. Groundwater circulation operates as a shallow crustal system dominated by meteoric recharge, structurally confined by fault architecture. Conversely, geothermal gases predominantly represent deep-seated fluids, with their high mobility and low density enabling efficient ascent through fractures. This explains why mantle/crustal signals are preserved in gases but attenuated in aqueous phases. To further constrain groundwater source area, we have calculated the thermal reservoir temperature of EAFZ groundwater, and the results are shown in Table S2. Due to the low water-rock interaction degree and diversity of rock types in this area, cations in water are difficult to reach water-rock equilibrium (Fig. 4). Hence, most of the cationic thermometer estimates are too large or too small, which can only be used as a reference for thermal reservoirs. Fortunately, SiO2 thermometers are relatively suitable for estimating the reservoir temperature. As can be seen from Table S2, the reservoir temperatures range from  $19.81^{\circ}\mathrm{C}$ to 128.09 °C (Quartz, no steam loss), which belongs to the low or moderate temperature geothermal systems. Using the circulation depth calculation formula, the maximum circulation depth is estimated to be 4.4km (HS04) (Table S2).

237

238

239

240

241

242

243

244

245

246

247248

249

250251

252

253

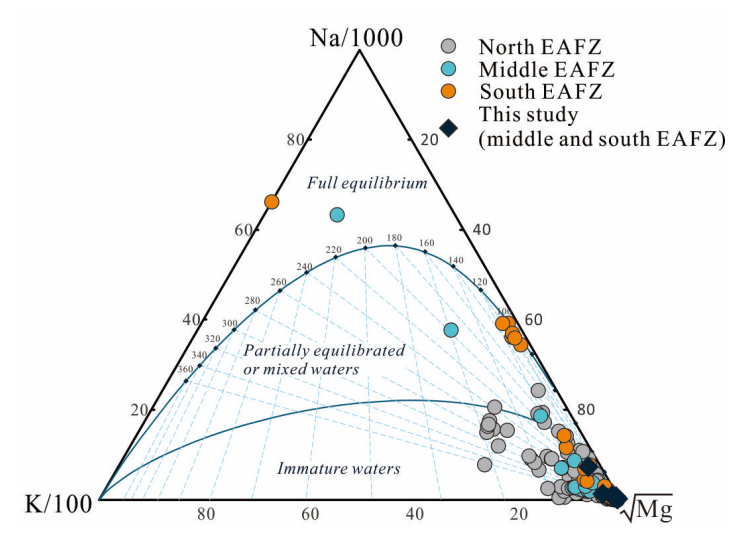


Fig. 4. Na-K-Mg ternary diagram of groundwaters in EAFZ. Literature data source is consistent with Fig. 2.

#### 5.1.3 87Sr/86Sr characteristics of groundwaters

Radiogenic strontium isotopes (87Sr/86Sr) serve as robust tracers of groundwater provenance. The measured 87Sr/86Sr ratios (0.7053–0.713) across EAFZ groundwaters reflect multi-source mixing processes. Central-southern groundwaters integrate signatures from: Shallow aquifers: Inheriting Sr from local lithologies (ophiolites) (Oyan, 2018); Modern seawater: 87Sr/86Sr = 0.7092–0.7096 (Mediterranean seawater) (Banner, 2004; Bernat et al., 1972); River inputs: Enriched ratios (>0.710) from silicate weathering. Binary mixing models using 87Sr/86Sr vs. Ca/Sr ratios (Fig. 5) quantify source contributions: Carbonate weathering dominates, consistent with Ca-HCO₃ hydrochemical type; Ophiolite contributions <10% (except Mg²+-rich samples near ultramafic outcrops); Evaporite dissolution contributes 0–20% (≤50% in localized high-SO₄²- zones). Sr isotope framework corroborates earlier findings of shallow-dominated circulation in central-southern EAFZ.

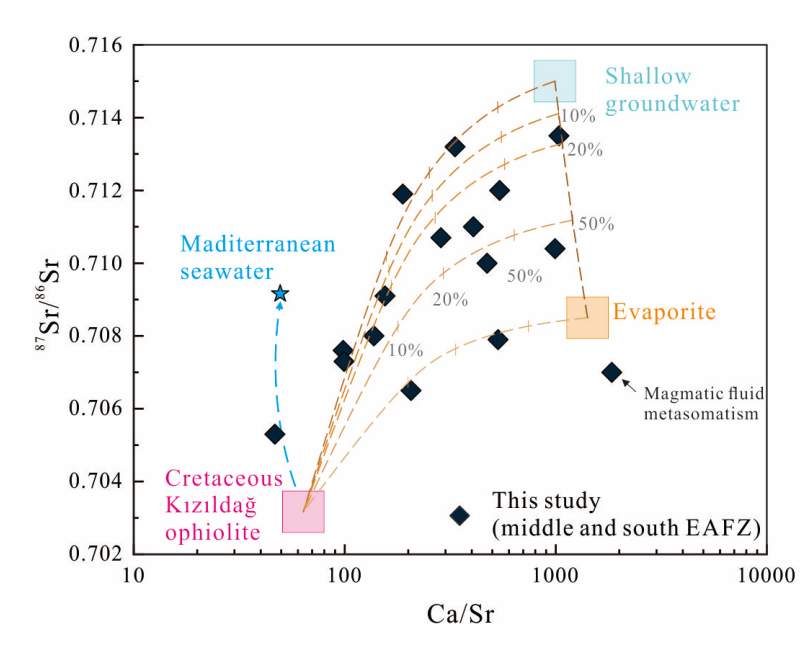


Fig. 5.  $^{87}$ Sr/ $^{86}$ Sr vs. Ca/Sr of groundwaters in the EAFZ. The mixing-boundary lines are built with the following end members: Mediterranean Sea water Ca = 411ppm, Sr = 8.30ppm  $^{87}$ Sr/ $^{86}$ Sr = 0.7092 (Banner, 2004; Bernat et al., 1972); Cretaceous Kızıldağ ophiolite CaO = 9.7%, Sr = 1088.10ppm  $^{87}$ Sr/ $^{86}$ Sr = 0.7032 (Oyan, 2018); Shallow groundwater (HS08) Ca = 55.34ppm, Sr = 0.06ppm  $^{87}$ Sr/ $^{86}$ Sr = 0.7150 (Affected by silicate weathering); Evaporite CaO = 29.5%, Sr = 149ppm  $^{87}$ Sr/ $^{86}$ Sr = 0.7085 (Güngör Yeşilova and Baran, 2023).

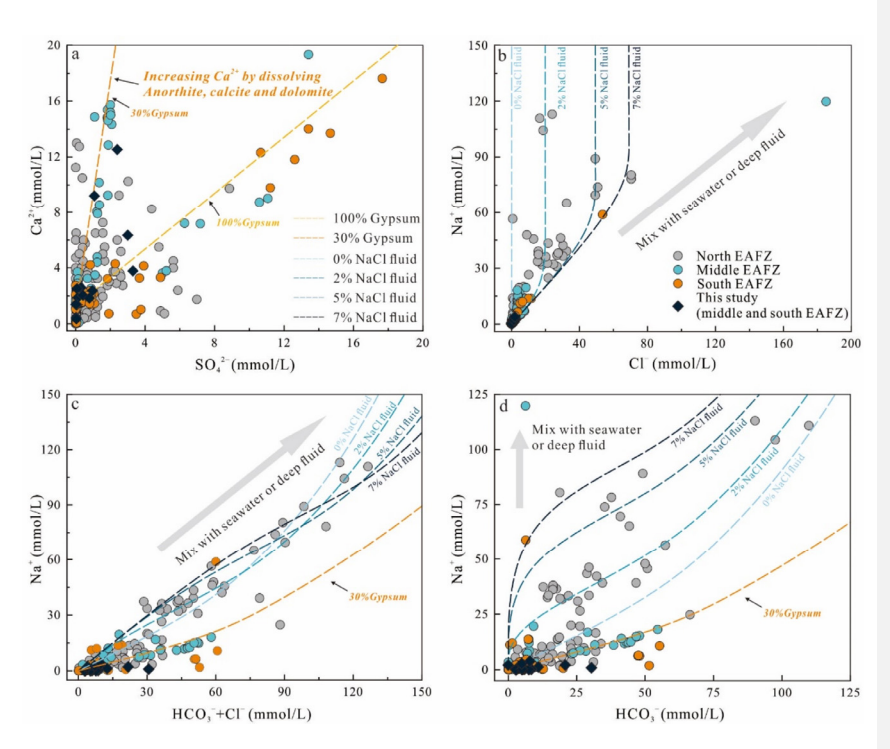


Fig. 6. Characteristics of chemical components of groundwaters in the EAFZ, during water-rock interaction. The dashed line is the numerical simulation result of PHREEQC. a:  $Ca^{2+}$  vs  $SO_4^{2-}$ , b:  $Na^+$  vs  $Cl^-$ , c:  $Na^+$  vs  $HCO_3^-+Cl^-$  and d:  $Na^+$  vs  $HCO_3^-$ . The simulation calculations are detailed in Supporting Information Part 1. Literature data source is consistent with Fig. 2.

 $5.2\ The$  groundwater circulation in different segments of EAFZ

### 5.2.1 Water-rocks interaction

 Pre-seismic whitish discoloration and turbidity anomalies observed at spring HS04 and well HS14, monitoring stations likely reflect seismically induced perturbations to water-rock equilibrium (Video 1 and 2). To validate this hypothesis, we conducted numerical simulations of water-rock interaction processes across distinct segments of EAFZ, aiming to reconstruct their hydrochemical evolution.

Fig. 6 indicates pronounced disparities in groundwater chemistry between northern and central-southern segments. As discussed, elevated Na<sup>+</sup> and Cl<sup>-</sup> concentrations in northern groundwaters suggest magmatic fluid contributions. During ascent, these deep-sourced Na-Cl rich fluids mix with shallow groundwater while reacting with surrounding rocks. To quantify magmatic mixing ratios and reaction pathways, we first characterized dominant lithologies in the northern EAFZ—basalt, basaltic andesite, and sedimentary

删除了: HS04 and HS14 groundwater

cover (clastics and carbonates). CIPW norm calculations were employed to estimate mineral abundances, followed by PHREEQC-based reactive transport modeling (Parkhurst and Appelo, 2013) (see Supplementary File 1 for parameters). Simulation results (Fig. 6) demonstrate that linear correlations between Na<sup>+</sup> and (HCO<sub>3</sub><sup>-</sup>+ Cl<sup>-</sup>) arise from magmatic NaCl fluid-carbonate interactions, with magmatic contributions accounting for 0–7% of total mixing.

In contrast, central–southern groundwaters lack magmatic signatures but exhibit Ca<sup>2+</sup>–SO<sub>4</sub><sup>2-</sup> covariation indicative of anhydrite dissolution (Fig. 6). Central segment waters reflect mixed carbonate- anhydrite controls (30% anhydrite contribution), while southern systems are dominated by anhydrite-derived solutes (100%), sourced from extensive evaporite deposits of the paleo–Amik Lake. Silica–enthalpy mixing models estimate reservoir temperatures of 234°C (HS04) and 155°C (HS14) (Fig. 7a), underwhich anhydrite saturation indices confirm its dissolution dominance (Fig. 7b). Notably, HS14—located 20 km from the paleo–Amik Basin—displayed prominent pre-seismic turbidity anomalies, likely triggered by earthquake-driven disruption of anhydrite equilibrium. Coseismic changes in temperature, pressure, fracture density, and circulation depth may have enhanced evaporite dissolution, increasing groundwater salinity.

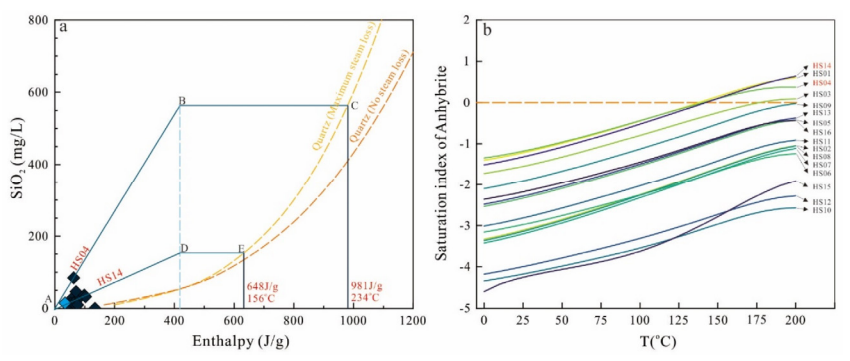


Fig. 7. a: Silica-enthalpy model of groundwaters in EAFZ. b: Temperature versus variation of anhydrite saturation indices of groundwaters in EAFZ. The enthalpies and reservoir temperatures of sample HS04 and HS14 are 981 J/g, 234 °C and 648 J/g, 156 °C respectively. The blue diamond is sample HS08, which is river water. At reservoir temperature, the anhydrite in HS04 and HS14 samples is saturated, indicating that anhydrite dissolution occurs during the water-rock reaction.

5.2.2 Contribution of mantle degassing to EAFZ groundwater circulation

Geochemical studies of EAFZ geothermal gases indicate significant mantle degassing (Fig. 8), where sulfur volatiles (e.g.,  $SO_2$  and  $H_2S$ ) ascend through fault conduits and oxidize upon mixing with shallow

删除了: HS04

删除了: groudwaters

groundwater, ultimately mobilizing as  $SO_4^{2^-}$  in thermal fluids. Consequently, mantle-derived sulfur contributions to groundwater sulfate inventories cannot be disregarded. Lacking  $O_2$  was detected in EAFZ geothermal gases suggested that the dissolved oxygen may have been consumed (Italiano et al., 2013; Yuce et al., 2014). However, it is important to note that  $H_2S$ ,  $H_2$ , and  $CH_4$  can all react with oxygen. Thermodynamic calculations indicate that  $CH_4$  is more favorable than  $H_2S$  in oxidation reactions ( $\Delta G^\circ$   $CH_4 = -818.1$  kJ/mol,  $\Delta G^\circ$   $H_2S = -494.2$  kJ/mol, at 298 K and 1atm). In actual geothermal systems, however, the depletion of  $H_2S$  is more commonly observed than the depletion of  $CH_4$ . We propose the following possible explanations: 1) Oxidation of  $H_2S$ : While thermodynamic calculations predict  $CH_4$  oxidation first, a small amount of  $H_2S$  might still be oxidized simultaneously with  $CH_4$ . Due to the much lower concentration of  $H_2S$  in geothermal systems compared to  $CH_4$ ,  $H_2S$  is consumed more quickly, leaving  $CH_4$  with a higher residual concentration. 2) Exogenous  $CH_4$  Supply: In addition to mantle-derived  $CH_4$ , other sources of  $CH_4$ , such as biogenic  $CH_4$  and thermogenic  $CH_4$  (e.g., serpentinization), may contribute to the geothermal system. These external sources could increase the concentration of  $CH_4$  in the geothermal fluids.

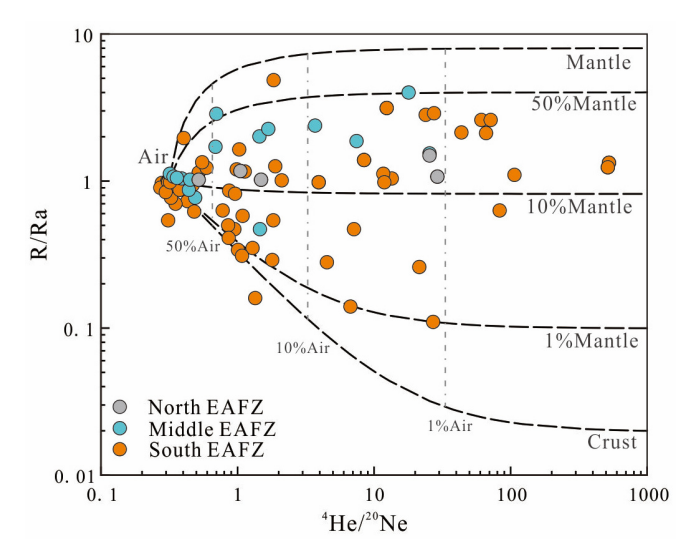


Fig. 8. Helium isotope ratios (R/Ra, Ra = air  $^3$ He/ $^4$ He = 1.39 × 10 $^4$ 6) versus  $^4$ He/ $^2$ 0Ne ratios for EAFZ gas samples. The mixing-boundary lines are built with the following end members: Air R/Ra = 1 and  $^4$ He/ $^2$ 0Ne = 0.318; mantle R/Ra = 8 and  $^4$ He/ $^2$ 0Ne = 1000; continental crust R/Ra = 0.02 and  $^4$ He/ $^2$ 0Ne = 1000 (Sano and Wakita, 1985). Literature data source from (D'Alessandro et al., 2018; Inguaggiato et al., 2016; Italiano et al., 2013; YASİN and YÜCE, 2023; Yuce et al., 2014; Yuce and Taskiran, 2013).

However, previous studies have shown that the geothermal gas in the southern segment of EAFZ has more crustal source components than northern segment (Fig. 8). Furthermore, isotopic evidence confirms substantial biogenic and serpentinization-derived CH<sub>4</sub> inputs (Italiano et al., 2013; Yan et al., 2024), whereas H<sub>2</sub>S remains below detection thresholds. This implies that while H<sub>2</sub>S may transiently influence redox cycling, its low abundance limits long-term impacts. Instead, post-seismic SO<sub>4</sub><sup>2-</sup> surges likely originate from shallow evaporite dissolution (anhydrite) or low-temperature metamorphic anhydrite hydration—processes amplified by coseismic fracture propagation and fluid remobilization. 5.3 Geothermal fluid circulation model in the EAFZ As discussed above, EAFZ's geothermal fluid circulation model is shown in the Fig. 9. Beginning in the Late Cretaceous, as the New Tethys Ocean closed, Arabia-Eurasia collision zone have accommodated ~350 km of convergence, making crust up to 45 km thick, and causing >2 km of uplift (Yönlü et al., 2017). Arabian lithospheric mantle extends 50~150 km north beneath Anatolian crust (Whitney et al., 2023). Subsequently, the "roll back" and "slab break" occurred, resulting in extensive volcanic and devastating earthquakes, including those of February 6, 2023 in East Anatolian Plateau (Zhou et al., 2024). The collision of the Eurasian and Arabian plates caused Anatolian microplate was extruding westwards, which lead to EAFZ at a high strike-slip rate of ~11 mm/yr (Pousse - Beltran et al., 2020), and accompanied by counterclockwise rotation with a rotation rate of  $1.053\pm0.015^{\circ}/Ma$  (Simão et al., 2016). In this tectonic context, EAFZ remains active for a long time. Paleoseismic studies have shown that EAFZ has had many large earthquakes in its history (Carena et al., 2023; Hubert-Ferrari et al., 2020; Sparacino et al., 2022; Tan et al., 2008; Yönlü et al., 2017), with the largest magnitude reaching Mw 8.2 (Carena et al., 2023). Fault that cut through the crust provide channels for material and energy to rise up from mantle, which makes EAFZ geothermal gas contain a high proportion of mantle-derived compositions (Aydin et al., 2020; Italiano et al., 2013; Yuce et al., 2014). However, the transport of geothermal gas and geothermal water appears to be decoupled. On the one hand, deep geothermal fluid stays deep under the influence of gravity and less diffusive, compare to geothermal gas. On the other hand, the geothermal fluid was diluted due to the infiltration of a large

337

338

339340

341

342

343

344

345

346

347

348

349

350

351

352

353 354

355

356357

358

359

360

361

362

363

364 365 amount of shallow cold water after the double earthquakes in February 2023 (Mw 7.8 and Mw 7.6). Our interpretation can better explain the lack of deep fluid signal in the groundwater studied in this study.

surface and discharged into the atmosphere. On the contrary, the circulating groundwater has undergone complex water-rock interaction processes such as anhydrite, calcite, dolomite, anorthite and serpentinization (Fig. 9).

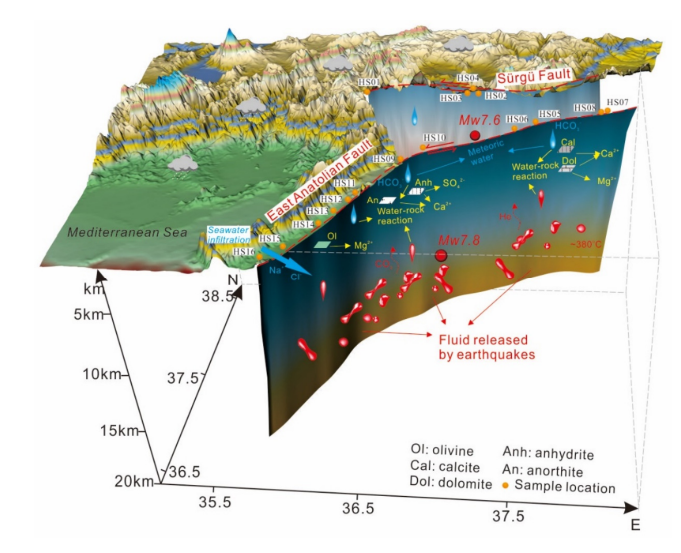


Fig. 9. The genesis model of the geothermal fluids in the EAFZ. The deep geothermal fluid was diluted due to the infiltration of a large amount of shallow cold water. In the shallow crust, gas-water interaction process and water-rock interaction processes were experienced. The gases rose to the surface and discharged into the atmosphere. The circulating groundwater has undergone complex such as anhydrite, calcite, dolomite, anorthite and serpentinization.

5.4 The relationship between geothermal fluid and earthquake forecasting

Earthquake forecasting is a grand goal pursued by human beings, but also one of the most difficult goals. Various physical, chemical and biological techniques are used for earthquake forecasting (Bayrak et al., 2015; Güleç et al., 2002; Jordan et al., 2011; Kwiatek et al., 2023; Kwiatek et al., 2023; Luo et al., 2024; Luo et al., 2023; Miller et al., 2004; Nalbant et al., 2002; Skelton et al., 2014; Tsunogai and Wakita, 1995; Wakita et al., 1980). As a link between the shallow (crust) and the deep (mantle), geothermal fluids can react to various diseases just like human blood. In earlier studies, researchers found that the anomaly of chemical indicators in geothermal fluids could be used for earthquake forecasting e.g., (Güleç et al., 2002; King et al., 2006; Miller et al., 2004; Perez et al., 2008; Poitrasson et al., 1999; Tsunogai and Wakita, 1995), but due to limited technology and funding, such research requiring long-term and large-scale monitoring is difficult to carry out (Ingebritsen and Manga, 2014). With the advancement of

technology, more and more automated equipment and the development of 5G communication technology make long-term automatic monitoring possible, e.g., (Barbieri et al., 2021; Boschetti et al., 2022; Franchini et al., 2021; Liang et al., 2023; Luo et al., 2024; Luo et al., 2023; Skelton et al., 2014; Wang et al., 2023a). However, before geothermal fluid is really used in earthquake prediction, there is a problem that must be solved (i.e. to understand the relationship between geothermal fluid and earthquake). Its essence is to restore the origin and evolution process of geothermal fluid (Boschetti et al., 2022). For a long time, researchers have been searching for the information of the deep fluid in the fault zone, trying to link the earthquake with the deep fluid activity (Liang et al., 2023; Luo et al., 2023; Yan et al., 2024). However, deep information is easily changed during upward migration, and sometimes even lacks deep information, just like the EAFZ groundwater in this study (Fig. 6). This seems to limit the ability of groundwater to be used for earthquake prediction. In fact, chemical anomalies related to seismic activity can still be found in some shallow circulating groundwater (e.g., SO<sub>4</sub><sup>2-</sup>) (Luo et al., 2023). Moreover, the shallower water-rock interactions are more sensitive to the environment. Shallowcirculation water-rock interactions are fundamentally controlled by host rock lithology, where distinct lithologic units impart unique hydrochemical signatures to circulating fluids—enabling specific strata to function as target indicator horizons for tracing seismotectonic hazards. Groundwater-rock systems typically maintain equilibrium under stable conditions, but external perturbations (e.g., seismic stress or rainfall variability) can disrupt regional hydrogeochemical equilibria, accelerate dissolution of target horizons like evaporites, and amplify water-rock interaction intensity, thereby generating diagnostic solute anomalies. For instance, anhydrite dissolution manifests as covariant Ca<sup>2+</sup>-SO<sub>4</sub><sup>2-</sup> anomalies; accelerated dissolution from seismic/seasonal forces triggers synchronous Ca-SO<sub>4</sub><sup>2-</sup> concentration spikes and salinity increases, producing macroscopic turbidity or whitening. Consequently, analyzing regional hydrogeochemical baselines to identify aquifer-specific target horizons, implementing their continuous monitoring, and establishing localized evaluation thresholds enables early warning systems for geohazard precursors. Anhydrite are widely distributed in nature, and its formation is related to evaporite or hydrothermal metasomatism. Dissolution and precipitation of anhydrite are often observed in groundwater. Its solubility is greatly affected by environmental conditions (temperature, pH, pressure surrounding rock condition etc.) and they are potential indicators of tectonic activity (Jin et al., 2016). After the 2023 Mw 7.8 and 2023 Mw 7.6 earthquake, in the absence of deep fluid signals, we observed anhydrite dissolution

386

387

388 389

390

391

392

393

394

395

396

397 398

399

400

401

402

403

404

405

406

407

408 409

410

411

412

413

414

at central-southern segments of EAFZ, which are likely to have been affected by seismic activity (Fig. 6). Similar SO<sub>4</sub><sup>2-</sup> anomalies have also been found in the eastern Tibetan Plateau (Li et al., 2021; Luo et al., 2023) and southeast China (Wang et al., 2021). Therefore, we suggest that anhydrite can be used as a potential tectonic activity index. However, although anhydrite's potential as a tectonic activity proxy is significant, its shallow crustal occurrence renders it susceptible to climatic perturbations (e.g., rainfall, evaporation). As evidenced in Fig. 6, post-seismic SO<sub>4</sub><sup>2-</sup> and Ca<sup>2+</sup> concentrations show no statistically significant deviations from background levels during quiescent periods, underscoring the challenge of filtering out climatic noise. While statistical correlations tentatively position anhydrite dissolution as a fault activity indicator, advancing this paradigm requires: Long-term, high-resolution monitoring to disentangle tectonic vs. meteoric signals (e.g., Thermal-hydrothermal experimental and statistical or machine learning approaches (e.g., PCA, random forests)); Mechanistic models integrating fracture permeability dynamics with anhydrite solubility kinetics. This study's key contribution lies in establishing fault-driven permeability changes as a viable driver of anhydrite dissolution. We propose a novel conceptual framework for fault activity monitoring via groundwater systems—one that prioritizes reactive minerals in shallow water-rock interactions over traditional deep fluid signals. **6 Conclusions** Segmented groundwater provenance: Northern groundwaters represent mixing between mantle-derived magmatic fluids (0-7%) and shallow meteoric waters, while central-southern systems are dominated by carbonate-evaporite weathering with localized seawater/halite inputs. Tectono-Climatic controls on water-rock interactions: Plagioclase-carbonate dissolution dominates northern segments, whereas anhydrite dissolution (30-100%) in central-southern segments correlates with fault permeability changes. Seismically enhanced fracture networks amplify evaporite dissolution, driving hydrochemical anomalies. Anhydrite as a tectonic activity tracer: Despite climatic noise, anhydrite dissolution kinetics exhibit stress-state sensitivity. Their ubiquity and rapid stress response position anhydrite as a potential tracer

416

417

418

419

420

421

422

423

424

425

426

427

428

429

430

431

432

433

434

435

436

437

438

439 440

441

442

443

for real-time fault activity monitoring.

The fundamental contribution of this study lies in proposing a novel research paradigm: identifying suitable target indicator horizons. Regionally variable minerals may serve as diagnostic tracers. By analyzing the regional hydrogeochemical context to elucidate groundwater circulation and water-rock interaction mechanisms, we can identify optimal target horizons for specific areas, implement continuous monitoring, establish region-specific evaluation metrics, thus achieving early warning capabilities for seismically induced geohazards.

450	Code and data availability. All water data are listed in the text or in the Supporting Information.
451	Supplement. See Supporting Information.
452	Authorship contributions. Zebin Luo: Conceptualization, Methodology, Software, Writing-Original
453	Draft, Writing-Review and Editing. Xiaocheng Zhou: Conceptualization, Validation. Yueren Xu:
454	Investigation. Peng Liang: Investigation. Huiping Zhang: Investigation. Jinlong Liang: Validation.
455	Zhaojun Zeng: Investigation. Yucong Yan: Investigation. Zheng Gong: Investigation. Shiguang Wang
456	Investigation. Chuanyou Li: Investigation. Zhikun Ren: Investigation. Jingxing Yu: Investigation.
457	Zifa Ma: Investigation. Junjie Li: Investigation.
458	Competing Interests. The authors declare that they have no known competing financial interests or
459	personal relationships that could have appeared to influence the work reported in this paper.
460	Acknowledgements. We would like to thank the Associate Editor Prof. Heng Dai, Walter D'Alessandro
461	Giovanni Martinelli, Hafidha Khebizi and another anonymous reviewers for their constructive comments,
462	suggestions and corrections. We also thank Dr. Yinchun Wang Dr. Renjie Li and Dr. Yi Yu for discussion,
463	Dr. Shiqi Zhang for her help for diagram drawing.
464	Financial support. The work was funded by National Key Research and Development Project
465	(2024ZD1000503, 2023YFC3012005-1), Central Public-interest Scientific Institution Basal Research
466	Fund (CEAIEF20240405, CEAIEF2022030200, CEAIEF2022030205), the National Natural Science
467	Foundation of China (41673106, 4193000170), IGCP Project 724.

#### References

468

- 469 Aydin, H., Karakuş, H., and Mutlu, H.: Hydrogeochemistry of geothermal waters in
- 470 eastern Turkey: Geochemical and isotopic constraints on water-rock interaction,
- Journal of Volcanology and Geothermal Research, 390, 2020.
- 472 Baba, A., Şaroğlu, F., Akkuş, I., Özel, N., Yeşilnacar, M. İ., Nalbantçılar, M. T., Demir,
- 473 M. M., Gökçen, G., Arslan, Ş., Dursun, N., Uzelli, T., and Yazdani, H.: Geological and
- 474 hydrogeochemical properties of geothermal systems in the southeastern region of
- 475 Turkey, Geothermics, 78, 255-271, 2019.
- 476 Banner, J. L.: Radiogenic isotopes: systematics and applications to earth surface
- 477 processes and chemical stratigraphy, Earth-Science Reviews, 65, 141-194, 2004.
- 478 Barbieri, M., Franchini, S., Barberio, M. D., Billi, A., Boschetti, T., Giansante, L., Gori,
- 479 F., Jonsson, S., Petitta, M., Skelton, A., and Stockmann, G.: Changes in groundwater
- 480 trace element concentrations before seismic and volcanic activities in Iceland during
- 481 2010-2018, Science of the Total Environment, 793, 2021.
- 482 Bayrak, E., Yılmaz, Ş., Softa, M., Türker, T., and Bayrak, Y.: Earthquake hazard
- analysis for East Anatolian Fault Zone, Turkey, Natural Hazards, 76, 1063-1077, 2015.
- 484 Bernat, M., Church, T., and Allegre, C. J.: Barium and strontium concentrations in
- 485 Pacific and Mediterranean sea water profiles by direct isotope dilution mass
- spectrometry, Earth and Planetary Science Letters, 16, 75-80, 1972.
- 487 Bilim, F., Aydemir, A., Kosaroglu, S., and Bektas, O.: Effects of the Karacadag Volcanic
- 488 Complex on the thermal structure and geothermal potential of southeast Anatolia,
- Bulletin of Volcanology, 80, 2018.
- 490 Boschetti, T., Barbieri, M., Barberio, M. D., Skelton, A., Stockmann, G., and Toscani,
- 491 L.: Geothermometry and water-rock interaction modelling at Hafralkur: Possible
- 492 implications of temperature and CO2 on hydrogeochemical changes previously linked
- to earthquakes in northern Iceland, Geothermics, 105, 2022.
- 494 Bürgmann, R.: Reliable earthquake precursors?, Science, 381, 266-267, 2023.
- 495 Carena, S., Friedrich, A. M., Verdecchia, A., Kahle, B., Rieger, S., and Kübler, S.:
- 496 Identification of Source Faults of Large Earthquakes in the Turkey Syria Border
- 497 Region Between 1000 CE and the Present, and Their Relevance for the 2023 Mw 7.8
- 498 Pazarcık Earthquake, Tectonics, 42, 2023.
- 499 Craig, H.: Isotopic Variations in Meteoric Waters, Science, 133, 1702-1703, 1961.
- 500 D'Alessandro, W., Yüce, G., Italiano, F., Bellomo, S., Gülbay, A. H., Yasin, D. U., and
- 501 Gagliano, A. L.: Large compositional differences in the gases released from the
- 502 Kizildag ophiolitic body (Turkey): Evidences of prevailingly abiogenic origin, Marine
- and Petroleum Geology, 89, 174-184, 2018.
- 504 Franchini, S., Agostini, S., Barberio, M. D., Barbieri, M., Billi, A., Boschetti, T., Pennisi,
- 505 M., and Petitta, M.: HydroQuakes, central Apennines, Italy: Towards a
- 506 hydrogeochemical monitoring network for seismic precursors and the hydro-seismo-
- sensitivity of boron, Journal of Hydrology, 598, 2021.
- 508 Giggenbach, W. F.: Isotopic shifts in waters from geothermal and volcanic systems
- along convergent plate boundaries and their origin, Earth and Planetary Science Letters,
- 510 113, 495-510, 1992.

删除了:

- 512 Güleç, N. and Hilton, D. R.: Turkish geothermal fields as natural analogues of CO 2
- 513 storage sites: Gas geochemistry and implications for CO 2 trapping mechanisms,
- 514 Geothermics, 64, 96-110, 2016.
- 515 Güleç, N., Hilton, D. R., and Mutlu, H.: Helium isotope variations in Turkey::
- 516 relationship to tectonics, volcanism and recent seismic activities, Chemical Geology,
- 517 187, 129-142, 2002.
- 518 Güngör Yeşilova, P. and Baran, O.: Origin and Paleoenvironmental Conditions of the
- 519 Köprüağzı Evaporites (Eastern Anatolia, Turkey): Sedimentological, Mineralogical and
- 520 Geochemical Constraints, Minerals, 13, 282, 2023.
- 521 Hubert-Ferrari, A., Lamair, L., Hage, S., Schmidt, S., Çağatay, M. N., and Avşar, U.: A
- 3800 yr paleoseismic record (Lake Hazar sediments, eastern Turkey): Implications for
- 523 the East Anatolian Fault seismic cycle, Earth and Planetary Science Letters, 538, 2020.
- 524 Ingebritsen, S. E. and Manga, M.: EARTHQUAKES Hydrogeochemical precursors,
- 525 Nature Geoscience, 7, 697-698, 2014.
- 526 Inguaggiato, C., Censi, P., D'Alessandro, W., and Zuddas, P.: Geochemical
- characterisation of gases along the dead sea rift: Evidences of mantle-co2 degassing,
- Journal of Volcanology and Geothermal Research, 320, 50-57, 2016.
- 529 Italiano, F., Sasmaz, A., Yuce, G., and Okan, O. O.: Thermal fluids along the East
- 530 Anatolian Fault Zone (EAFZ): Geochemical features and relationships with the tectonic
- setting, Chemical Geology, 339, 103-114, 2013.
- 532 Jin, Z., West, A. J., Zhang, F., An, Z., Hilton, R. G., Yu, J., Wang, J., Li, G., Deng, L.,
- and Wang, X.: Seismically enhanced solute fluxes in the Yangtze River headwaters
- following the AD 2008 Wenchuan earthquake, Geology, 44, 47-50, 2016.
- 535 Jordan, T. H., Chen, Y.-T., Gasparini, P., Madariaga, R., Main, I., Marzocchi, W.,
- 536 Papadopoulos, G., Sobolev, G., Yamaoka, K., and Zschau, J.: Operational Earthquake
- 537 <u>Forecasting: State of Knowledge and Guidelines for Utilization, Annals of Geophysics,</u>
- 538 <u>54, 315-391, 2011.</u>
- 539 Karaoğlu, Ö., Bazargan, M., Baba, A., and Browning, J.: Thermal fluid circulation
- 540 around the Karliova triple junction: Geochemical features and volcano-tectonic
- implications (Eastern Turkey), Geothermics, 81, 168-184, 2019.
- 542 Karaoğlu, Ö., Browning, J., Salah, M. K., Elshaafi, A., and Gudmundsson, A.: Depths
- of magma chambers at three volcanic provinces in the Karlıova region of Eastern
- Turkey, Bulletin of Volcanology, 80, 2018.
- 545 Karaoğlu, Ö., Gülmez, F., Göçmengil, G., Lustrino, M., Di Giuseppe, P., Manetti, P.,
- 546 Savaşçın, M. Y., and Agostini, S.: Petrological evolution of Karlıova-Varto volcanism
- 547 (Eastern Turkey): Magma genesis in a transtensional triple-junction tectonic setting,
- 548 Lithos, 364-365, 2020.
- 549 King, C.-Y., Zhang, W., and Zhang, Z.: Earthquake-induced Groundwater and Gas
- Changes, Pure and Applied Geophysics, 163, 633-645, 2006.
- Kwiatek, G., Martinez-Garzon, P., Becker, D., Dresen, G., Cotton, F., Beroza, G. C.,
- 552 Acarel, D., Ergintav, S., and Bohnhoff, M.: Months-long seismicity transients preceding
- 553 the 2023 M(W) 7.8 Kahramanmaras earthquake, Turkiye, Nat Commun, 14, 7534, 2023.
- Lanari, R., Boutoux, A., Faccenna, C., Herman, F., Willett, S. D., and Ballato, P.:
- 555 Cenozoic exhumation in the Mediterranean and the Middle East, Earth-Science

- 556 Reviews, 237, 2023.
- 557 Li, C., Zhou, X., Yan, Y., Ouyang, S., and Liu, F.: Hydrogeochemical Characteristics of
- 558 Hot Springs and Their Short-Term Seismic Precursor Anomalies along the Xiaojiang
- Fault Zone, Southeast Tibet Plateau, Water, 13, 2021.
- 560 Liang, J., Yu, Y., Shi, Z., Li, Z., Huang, Y., Song, H., Xu, J., Wang, X., Zhou, X., Huang,
- 561 L., Luo, Z., Tong, J., and Zhai, W.: Geothermal springs with high δ13CCO2-DIC along
- 562 the Xianshuihe fault, Western Sichuan, China: A geochemical signature of enhanced
- deep tectonic activity, Journal of Hydrology, 623, 129760, 2023.
- 564 Liang, P., Xu, Y., Zhou, X., Li, Y., Tian, Q., Zhang, H., Ren, Z., Yu, J., Li, C., Gong, Z.,
- Wang, S., Dou, A., Ma, Z., and Li, J.: Coseismic surface ruptures of MW7.8 and MW7.5
- 566 earthquakes occurred on February 6, 2023, and seismic hazard assessment of the East
- 567 Anatolian Fault Zone, Southeastern Türkiye, Science China Earth Sciences, 68, 611-
- 568 625, 2024.
- 569 Liu, X., Dong, S., Yue, Y., Guan, Q., Sun, Y., Chen, S., Zhang, J., and Yang, Y.:
- 570 87Sr/86Sr isotope ratios in rocks determined using inductively coupled plasma tandem
- 571 mass spectrometry in O2 mode without prior Sr purification, Rapid Communications
- in Mass Spectrometry, 34, e8690, 2020.
- 573 Luo, Z., Yang, M., Zhou, X., Liu, G., Liang, J., Liu, Z., Hua, P., Ma, J., Hu, L., Sun, X.,
- Cui, B., Wang, Z., and Chen, Y.: Evaluation of Various Forms of Geothermal Energy
- 575 Release in the Beijing Region, China, Water, 16, 2024.
- 576 Luo, Z., Zhou, X., He, M., Liang, J., Li, J., Dong, J., Tian, J., Yan, Y., Li, Y., Liu, F.,
- Ouyang, S., Liu, K., Yao, B., Wang, Y., and Zeng, Z.: Earthquakes evoked by lower
- crustal flow: Evidence from hot spring geochemistry in Lijiang-Xiaojinhe fault, Journal
- 579 of Hydrology, 619, 129334, 2023.
- 580 Ma, Z., Li, C., Jiang, Y., Chen, Y., Yin, X., Aoki, Y., Yun, S. H., and Wei, S.: Space
- 581 Geodetic Insights to the Dramatic Stress Rotation Induced by the February 2023
- Turkey Syria Earthquake Doublet, Geophysical Research Letters, 51, 2024.
- 583 Maden, N. and Öztürk, S.: Seismic b-Values, Bouguer Gravity and Heat Flow Data
- Beneath Eastern Anatolia, Turkey: Tectonic Implications, Surveys in Geophysics, 36,
- 585 549-570, 2015.
- Miller, S. A., Collettini, C., Chiaraluce, L., Cocco, M., Barchi, M., and Kaus, B.:
- 587 Aftershocks driven by a high-pressure CO2 source at depth, Nature, 427, 724-727, 2004.
- Nalbant, S. S., McCloskey, J., Steacy, S., and Barka, A. A.: Stress accumulation and
- increased seismic risk in eastern Turkey, Earth and Planetary Science Letters, 195, 291-
- 590 298, 2002.
- 591 Okan, O. O., Kalender, L., and Cetindag, B.: Trace-element hydrogeochemistry of
- 592 thermal waters of Karakocan (Elazig) and Mazgirt (Tunceli), Eastern Anatolia, Turkey,
- Journal of Geochemical Exploration, 194, 29-43, 2018.
- 594 Över, S., Demirci, A., and Özden, S.: Tectonic implications of the February 2023
- Earthquakes (Mw7.7, 7.6 and 6.3) in south-eastern Türkiye, Tectonophysics, 866, 2023.
- 596 Oyan, V.: Petrogenesis of the Quaternary mafic alkaline volcanism along the African-
- 597 Anatolian plates boundary in Turunçlu-Delihalil (Osmaniye) region in southern Turkey,
- 598 Lithos, 314-315, 630-645, 2018.
- Özkan, A., Solak, H. İ., Tiryakioğlu, İ., Şentürk, M. D., Aktuğ, B., Gezgin, C., Poyraz,

- 600 F., Duman, H., Masson, F., Uslular, G., Yiğit, C. Ö., and Yavaşoğlu, H. H.:
- 601 Characterization of the co-seismic pattern and slip distribution of the February 06, 2023,
- 602 Kahramanmaraş (Turkey) earthquakes (Mw 7.7 and Mw 7.6) with a dense GNSS
- 603 network, Tectonophysics, 866, 2023.
- 604 Pan, S., Kong, Y., Wang, K., Ren, Y., Pang, Z., Zhang, C., Wen, D., Zhang, L., Feng,
- 605 Q., Zhu, G., and Wang, J.: Magmatic origin of geothermal fluids constrained by
- 606 geochemical evidence: Implications for the heat source in the northeastern Tibetan
- Plateau, Journal of Hydrology, 603, 2021.
- Parkhurst, D. L. and Appelo, C. A. J.: Description of input and examples for PHREEQC
- oo9 version 3: a computer program for speciation, batch-reaction, one-dimensional
- ${\it transport, and inverse geochemical calculations, U.S.\ Geological\ Survey,\ Reston,\ VA,}$
- 611 2013.
- 612 Pasvanoglu, S.: Geochemistry and conceptual model of thermal waters from Ercis -
- Zilan Valley, Eastern Turkey, Geothermics, 86, 2020.
- Perez, N. M., Hernandez, P. A., Igarashi, G., Trujillo, I., Nakai, S., Sumino, H., and
- Wakita, H.: Searching and detecting earthquake geochemical precursors in CO2-rich
- groundwaters from Galicia, Spain, Geochemical Journal, 42, 75-83, 2008.
- Poitrasson, F., Dundas, S. H., Toutain, J.-P., Munoz, M., and Rigo, A.: Earthquake-
- 618 related elemental and isotopic lead anomaly in a springwater, Earth and Planetary
- 619 Science Letters, 169, 269-276, 1999.
- 620 Pousse Beltran, L., Nissen, E., Bergman, E. A., Cambaz, M. D., Gaudreau, É.,
- 621 Karasözen, E., and Tan, F.: The 2020 Mw 6.8 Elazığ (Turkey) Earthquake Reveals
- Rupture Behavior of the East Anatolian Fault, Geophysical Research Letters, 47, 2020.
- 623 Sano, Y. and Wakita, H.: Geographical distribution of 3He/4He ratios in Japan:
- 624 Implications for arc tectonics and incipient magmatism, Journal of Geophysical
- Research: Solid Earth, 90, 8729-8741, 1985.
- 626 Simão, N. M., Nalbant, S. S., Sunbul, F., and Komec Mutlu, A.: Central and eastern
- Anatolian crustal deformation rate and velocity fields derived from GPS and earthquake
- data, Earth and Planetary Science Letters, 433, 89-98, 2016.
- 629 Skelton, A., Andren, M., Kristmannsdottir, H., Stockmann, G., Morth, C.-M.,
- 630 Sveinbjoernsdottir, A., Jonsson, S., Sturkell, E., Gudorunardottir, H. R., Hjartarson, H.,
- 631 Siegmund, H., and Kockum, I.: Changes in groundwater chemistry before two
- consecutive earthquakes in Iceland, Nature Geoscience, 7, 752-756, 2014.
- 633 Sparacino, F., Galuzzi, B. G., Palano, M., Segou, M., and Chiarabba, C.: Seismic
- 634 coupling for the Aegean Anatolian region, Earth-Science Reviews, 228, 2022.
- 635 Tan, O., Tapirdamaz, M. C., and Yoruk, A.: The earthquake catalogues for Turkey,
- Turkish Journal of Earth Sciences, 17, 405-418, 2008.
- 637 Tsunogai, U. and Wakita, H.: Precursory chemical changes in ground water: kobe
- 638 earthquake, Japan, Science (New York, N.Y.), 269, 61-63, 1995.
- van Hinsbergen, D. J. J., Gürer, D., Koç, A., and Lom, N.: Shortening and extrusion in
- 640 the East Anatolian Plateau: How was Neogene Arabia-Eurasia convergence tectonically
- accommodated?, Earth and Planetary Science Letters, 641, 2024.
- Wakita, H., Nakamura, Y., Kita, I., Fujii, N., and Notsu, K.: Hydrogen release: new
- indicator of fault activity, Science (New York, N.Y.), 210, 188-190, 1980.

- Wang, B., Zhou, X., Zhou, Y., Yan, Y., Li, Y., Ouyang, S., Liu, F., and Zhong, J.:
- 645 Hydrogeochemistry and Precursory Anomalies in Thermal Springs of Fujian
- 646 (Southeastern China) Associated with Earthquakes in the Taiwan Strait, Water, 13, 2021.
- 647 Wang, Y., Zhou, X., Tian, J., Zhou, J., He, M., Li, J., Dong, J., Yan, Y., Liu, F., Yao, B.,
- 648 Wang, Y., Zeng, Z., Liu, K., Li, L., Li, Z., and Xing, L.: Volatile characteristics and
- 649 fluxes of He-CO2 systematics in the southeastern Tibetan Plateau: Constraints on
- regional seismic activities, Journal of Hydrology, 617, 2023a.
- Wang, Z., Zhang, W., Taymaz, T., He, Z., Xu, T., and Zhang, Z.: Dynamic Rupture
- Process of the 2023 Mw 7.8 Kahramanmaraş Earthquake (SE Türkiye): Variable
- Rupture Speed and Implications for Seismic Hazard, Geophysical Research Letters, 50,
- 654 2023b.
- 655 Whitney, D. L., Delph, J. R., Thomson, S. N., Beck, S. L., Brocard, G. Y., Cosca, M.
- 656 A., Darin, M. H., Kaymakci, N., Meijers, M. J. M., Okay, A. I., Rojay, B., Teyssier, C.,
- 657 and Umhoefer, P. J.: Breaking plates: Creation of the East Anatolian fault, the Anatolian
- plate, and a tectonic escape system, Geology, 51, 673-677, 2023.
- 659 Yan, Y., Zhang, Z., Zhou, X., Wang, G., He, M., Tian, J., Dong, J., Li, J., Bai, Y., Zeng,
- 660 Z., Wang, Y., Yao, B., Xing, G., Cui, S., and Shi, Z.: Geochemical characteristics of hot
- 661 springs in active fault zones within the northern Sichuan-Yunnan block: Geochemical
- evidence for tectonic activity, Journal of Hydrology, 635, 2024.
- YASİN, D. and YÜCE, G.: Isotope and hydrochemical characteristics of thermal waters
- along the active fault zone (Erzin-Hatay/Turkey) and their geothermal potential,
- Turkish Journal of Earth Sciences, 32, 721-739, 2023.
- 666 Yönlü, Ö., Altunel, E., and Karabacak, V.: Geological and geomorphological evidence
- 667 for the southwestern extension of the East Anatolian Fault Zone, Turkey, Earth and
- 668 Planetary Science Letters, 469, 1-14, 2017.
- Yuce, G., Italiano, F., D'Alessandro, W., Yalcin, T. H., Yasin, D. U., Gulbay, A. H.,
- Ozyurt, N. N., Rojay, B., Karabacak, V., Bellomo, S., Brusca, L., Yang, T., Fu, C. C.,
- 671 Lai, C. W., Ozacar, A., and Walia, V.: Origin and interactions of fluids circulating over
- 672 the Amik Basin (Hatay, Turkey) and relationships with the hydrologic, geologic and
- tectonic settings, Chemical Geology, 388, 23-39, 2014.
- 674 Yuce, G. and Taskiran, L.: Isotope and chemical compositions of thermal fluids at
- Tekman Geothermal Area (Eastern Turkey), GEOCHEMICAL JOURNAL, 47, 423-
- 676 435, 2013.

- 677 Zeng, Z., Yang, L., Cui, Y., Zhou, X., He, M., Wang, Y., Yan, Y., Yao, B., Hu, X., Shao,
- 678 W., Li, J., and Fu, H.: Assessment of geothermal waters in Yunnan, China: Distribution,
- quality and driving factors, Geothermics, 130, 103323, 2025.
- 680 Zhou, Z., Thybo, H., Artemieva, I. M., Kusky, T., and Tang, C.-C.: Crustal melting and
- 681 continent uplift by mafic underplating at convergent boundaries, Nature
- 682 Communications, 15, 2024.